ACS OMEGA

http://pubs.acs.org/journal/acsodf

Article

In Vitro Reconstitution and Analysis of SARS-CoV-2/Host Protein−Protein Interactions

Shayli Varasteh Moradi, Yue Wu, Patricia Walden, Zhenling Cui, Wayne A. Johnston, Dmitri Petrov, and Kirill Alexandrov*

Cite This: *ACS Omega* 2023, 8, 25009−25019

Read Online

ACCESS | Metrics & More | Article Recommendations | Supporting Information

ABSTRACT: The emergence of viral threats such as Ebola, ZIKA, and severe acute respiratory syndrome coronavirus-2 (SARS-CoV-2) requires a rapid and efficient approach for elucidating mechanisms of pathogenesis and development of therapeutics. In this context, cell-free protein synthesis (CFPS) holds a promise to resolve the bottlenecks of multiplexed protein production and interaction analysis among host and pathogen proteins. Here, we applied a eukaryotic CFPS system based on *Leishmania tarentolae* extract (LTE) protein expression in combination with AlphaLISA proximity-based protein interaction technology to identify intraviral and viral-human protein interactions of SARS-CoV-2 virus that can potentially be targeted by the existing or novel antiviral therapeutics. We produced and tested 54 putative human-viral protein pairs *in vitro* and identified 45 direct binary protein interactions. As a casing example of the assay's suitability for drug development applications, we analyzed the effect of a putative biologic on the human angiotensin-converting enzyme 2/receptor-binding domain (hACE2/RBD) interaction. This suggests that the presented pathogen characterization platform can facilitate the development of new therapeutic agents.

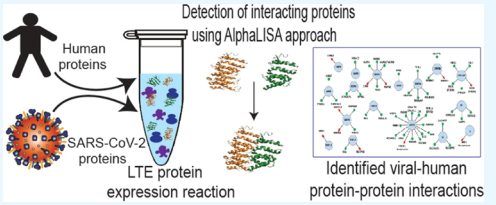

INTRODUCTION

The airborne coronavirus (severe acute respiratory syndrome coronavirus-2, SARS-CoV-2) is a causative agent of a global pandemic declared by WHO in March 2020.[1] SARS-CoV-2 is an enveloped virus with a positive-sense single-stranded RNA of around 30 kb in length that belongs to the *Coronaviridae* family (genus *betacoronavirus*).[2,3] The full-length genome sequence isolated at the early stage of the pandemic showed 79.6% sequence identity to the SARS-CoV virus.[3] Its RNA genome at the 5′ end contains two large open reading frames, ORF1a and ORF1b, occupying two-thirds of the genome. These two ORFs encode 16 nonstructural proteins (NSP1−NSP16) as a polyprotein (Figure 1A).[4,5] Processing of these NSPs leads to the formation of a replication−transcription complex (RTC) required for viral replication. As such, NSP3 and NSP5 encode for Papain-like protease (PLP) and 3CL-protease, which are responsible for the cleavage of the viral polyprotein and suppression of the host immune response, respectively. NSP12 and NSP15 encode RNA-dependent RNA polymerase (RdRp) and poly U-specific endoribonuclease, respectively.[5,6] NSP13 has the most conserved sequence among coronaviruses, and it is crucial for viral replication possessing RNA helicase and nuclease triphosphatase activities.[7] Four structural proteins (spike (S), envelope (E), membrane (M), and nucleocapsid (N)) proteins are transcribed from the 3′ end of the genome. In addition, nine putative ORFs encode accessory factors distributed among the structural protein coding region at the 3′ end of the genome (Figure 1A), bringing the total number of putative ORFs to 29. It is postulated that the accessory proteins in coronaviruses may not be required for virus replication but are associated with host manipulation.[8]

Protein interactions between viral and host proteins play a key role in viral replication and pathogenesis. Therefore, mapping host−virus protein−protein interactions is expected to provide insight into molecular mechanisms of pathogenesis and potentially reveal new drug targets. While mass spectrometry and yeast two-hybrid screening have been used extensively to construct putative interaction maps and were used successfully in the case of SARS-CoV-2,[9−13] the experimental validation of such a dense protein−protein interaction network represents a formidable challenge. Both the recombinant expression of hundreds of candidate proteins and their interaction analysis using conventional biophysical methods are prohibitive in terms of the cost and effort required. Some of these problems can be overcome by harnessing the power of high-throughput protein−protein interaction-based survival assays such as yeast two-hybrid systems.[12] However, the interaction of candidate proteins with yeast biochemistry may lead to artefacts, and therefore, as with

Received: March 9, 2023
Accepted: June 23, 2023
Published: July 6, 2023

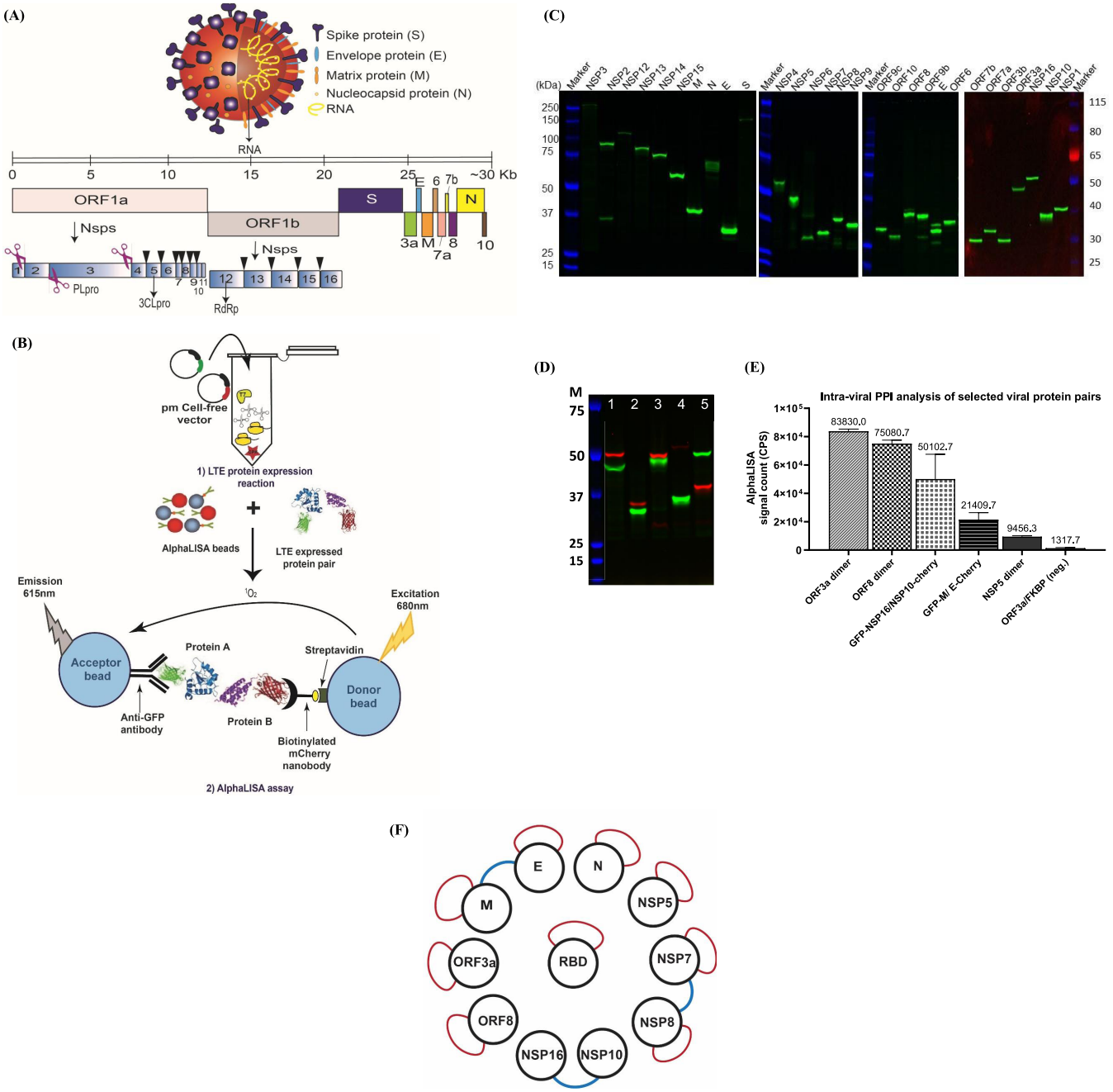

Figure 1. *In vitro* expression and protein−protein interaction analysis of selected SARS-CoV-2 ORFs. (A) Schematic representation of the SARS-CoV-2 virion structure and organization of its polycistronic genome. (B) Schematic overview of the *in vitro* protein−protein interaction analysis platform. The proteins co-expressed in LTE are captured by AlphaLISA beads, and the alpha signal is measured when the beads are brought into close proximity upon protein−protein interactions resulting in a luminescent signal (C) Fluorescent scan of the sodium dodecyl-sulfate (SDS-PAGE) gel loaded with the N-terminally eGFP-tagged SARS-CoV-2 proteins expressed in the LTE expression system. The expected molecular weights produced by proteins are reported in Table S1. (D) SDS-PAGE gel image of viral proteins tagged with either eGFP or mCherry co-expressed in the LTE lysate. Lane 1: ORF3 dimer, lane 2: ORF8 dimer, lane 3: NSP5 dimer, lane 4: eGFP-NSP10/NSP16-mCherry, and lane 5: eGFP-NSP16/NSP10-mCherry. (E) Plot of AlphaLISA signals of the protein−protein interaction assay for selected viral protein pairs. Samples were prepared in triplicate, and the data shows the average of the alpha signal obtained from each triplicate. (F) Protein−protein interaction map of selected intraviral protein interactions. Red curved lines and blue lines denote the detected homo- and heterodimers, respectively.

other approaches, the results of such screens require validation by alternative methods.[13−15]

Cell-free protein expression methods provide a powerful alternative for the production of large sets of complex eukaryotic proteins and their rapid interaction analysis.[16] In addition to excellent multiplexing capacity, this approach also mitigates problems associated with cytotoxic products and complexities arising from the need to co-express multiple ORFs.[17] The open environment of the *in vitro* translation reaction allows direct manipulation of the system by the introduction or removal of reaction components in a pre-, co-, or post-translational fashion. We developed and optimized a eukaryotic cell-free expression system based on the protozoan *L. tarentolae*.[18,19] The LTE cell-free expression platform takes

https://doi.org/10.1021/acsomega.3c01625
ACS Omega 2023, 8, 25009−25019

advantage of the eukaryotic *L. tarentolae* cell lysate supplemented with T7-based transcriptional machinery that generates mRNA templates for the endogenous translational machinery. To achieve efficient translation initiation in the LTE system, the DNA templates are furnished with a 5′ species-independent translational sequence (SITS).[20] Translation of endogenous mRNAs is suppressed by the introduction of antisense oligonucleotide targeting a short 5′ splice leader sequence of endogenous mRNAs. Benchmarking of LTE against several leading cell-free systems demonstrated that it is capable of producing large human proteins in full-length and monodispersed form on par with mammalian cell-free systems.[21] In our recent study, we showed the significant potential of LTE to produce folded proteins owing to co-translational chaperon assistance inherent to eukaryotic systems in contrast to the bacterial system.[22]

We subsequently expanded the platform by coupling it to high-throughput protein−protein interaction analysis known as the amplified luminescent proximity homogeneous assay screen (AlphaLISA).[23] It is a proximity bead-based assay in which a luminescent signal is generated when the acceptor and donor beads come into proximity as a result of the interaction of molecules attached to their surface. The assay does not require protein purification and, therefore, can utilize recombinant proteins in cell-free expression systems. Using this approach for analysis of protein−protein interactions requires 4 h protein expression and 1.5 h for the AlphaLISA assay. Multiplexing capability, where the analysis can be carried out in 384-well plates, makes this method particularly suitable for the analysis of protein interaction networks (Figure 1B).[24,25] As a proof of concept, we previously performed mapping of protein−protein interactions within the ZIKA virus proteome.[26]

Here, we report the reconstitution and analysis of 54 putative protein−protein interactions between the SARS-CoV-2 virus and human proteins previously identified by mass spectrometry and proposed to be druggable targets.[9] In addition, we reconstituted the direct interaction between the virus receptor-binding domain (RBD) variants and the human angiotensin-converting enzyme 2 (hACE2) *in vitro*. We evaluated the ability of anti-RBD antibodies to inhibit the RBD/hACE2 interaction and propose that the developed system can be used for antibody screening.

RESULTS

Expression of the SARS-CoV-2 Proteome in the LTE System and Its Functional Analysis. In order to understand the organization of the SARS-CoV-2 virus and its interaction with mammalian cells, we set out to perform systematic mapping of intraviral protein−protein interactions. The synthetic versions of SARS-CoV-2 ORF-coding sequences were inserted into multihost pmCell-Free vectors that enable protein expression in any cell-free systems or in mammalian cells.[26] The viral ORFs (Table S1) were cloned in a frame with N-terminal eGFP or C-terminal mCherry, which enables the expression of fluorescent fusion proteins both *in vitro* and in mammalian cell lines (Figures 1C and S3).

Initially, 28 viral genes were individually expressed in the LTE system as N-terminal GFP or C-terminal mCherry fusion proteins. The unboiled expression reactions were resolved on the SDS-PAGE gel, and the fluorescence of fusion proteins was detected and quantified by fluorescence scanning of the gels (Figures 1C and S1A). The concentration of eGFP-tagged proteins in the translation reactions was estimated to be in the 50−300 nM range (Figure S2). The viral proteins with a molecular weight of between 40 and 90 kDa were produced at higher levels, and the lowest yields were obtained for larger S and NSP3 proteins that have a molecular weight of 173 and 294.5 kDa, respectively.

To validate the protein interaction platform and the functionality of the *in vitro*-produced proteins, we analyzed the interactions of previously described 17 viral protein pairs including nine putative homodimers and eight heterodimers. Based on our previous study, we set a threshold of 1×10^4 counts per second (CPS) of the AlphaLISA signal as a cutoff for the positive interaction based on our previous study.[26] The positive alpha signals ranged between 1×10^4 and 8.3×10^4 CPS, and the negative control signal was 3.4×10^3 CPS (Table S4).

Positive alpha signals were obtained for 12 interactions, and four tested pairs produced negative signals (Figure 1D−F). The highest interaction signal in viral protein pairs was obtained for the ORF3a homodimer (8.3×10^4 CPS), whereas a marginal alpha signal (9.4×10^3 CPS) was observed for the NSP5 homodimer. Previous studies showed that the N-terminal finger residue of the NSP5 monomer is a critical interaction interface.[27,28] It is possible that N-terminal eGFP could sterically obstruct the N-terminal domain of a monomer and preclude dimer formation.

The interactions identified in this study were previously reported, which confirms that the LTE-expressed proteins were functional, and the assay could efficiently detect their interactions.[29−33] For instance, the crystal structure of the NSP10-NSP16 complex involved in viral RNA capping has been revealed earlier, and this complex formation is required to activate the 2′-*O*-methyltrasferase function of the NSP16 protein.[34,35] In our assay, the alpha signal intensity obtained for this complex was 5×10^4 CPS, which was 25× higher than the background signal.

The protein interactions of NSP7−NSP8 and NSP7 dimers were identified in our LTE system, whereas no interaction could be detected for NSP12−NSP7 and NSP12−NSP8 pairs. This may imply that all three proteins are required for the formation of the ternary NSP12−NSP7−NSP8 complex or that NSP12 produced in the LTE system was nonfunctional. It was previously reported that RNA-dependent RNA polymerase (NSP12) has only minimal activity on its own, while NSP7−NSP8 performs a cofactor role in stimulating its polymerase activity.[36] The cryo-EM structural analysis of SARS-CoV-2 NSP12 revealed the binding of an NSP8 monomer and an NSP7−NSP8 pair to this protein and the formation of an active protein complex.[37]

The homodimer formation of the wild-type RBD could also be confirmed using the LTE-expressed protein, resulting in an alpha signal of 2.9×10^4 CPS. This is consistent with a previous report on the structure of RBD bound to the hACE2 receptor.[38]

Interaction Analysis of *In Vitro* Expressed Human and SARS-CoV-2 Interacting Proteins. Gordon et al. reported 66 potential druggable human proteins that putatively interact with SARS-CoV-2 polypeptides.[9] We selected 56 of those proteins to experimentally validate their interaction with viral partners using the LTE system for their production. First, N-terminal eGFP and C-terminal mCherry fusions of putative human SARS-CoV-2 interacting proteins were expressed in LTE individually to confirm the integrity. From the selected

https://doi.org/10.1021/acsomega.3c01625
ACS Omega 2023, 8, 25009−25019

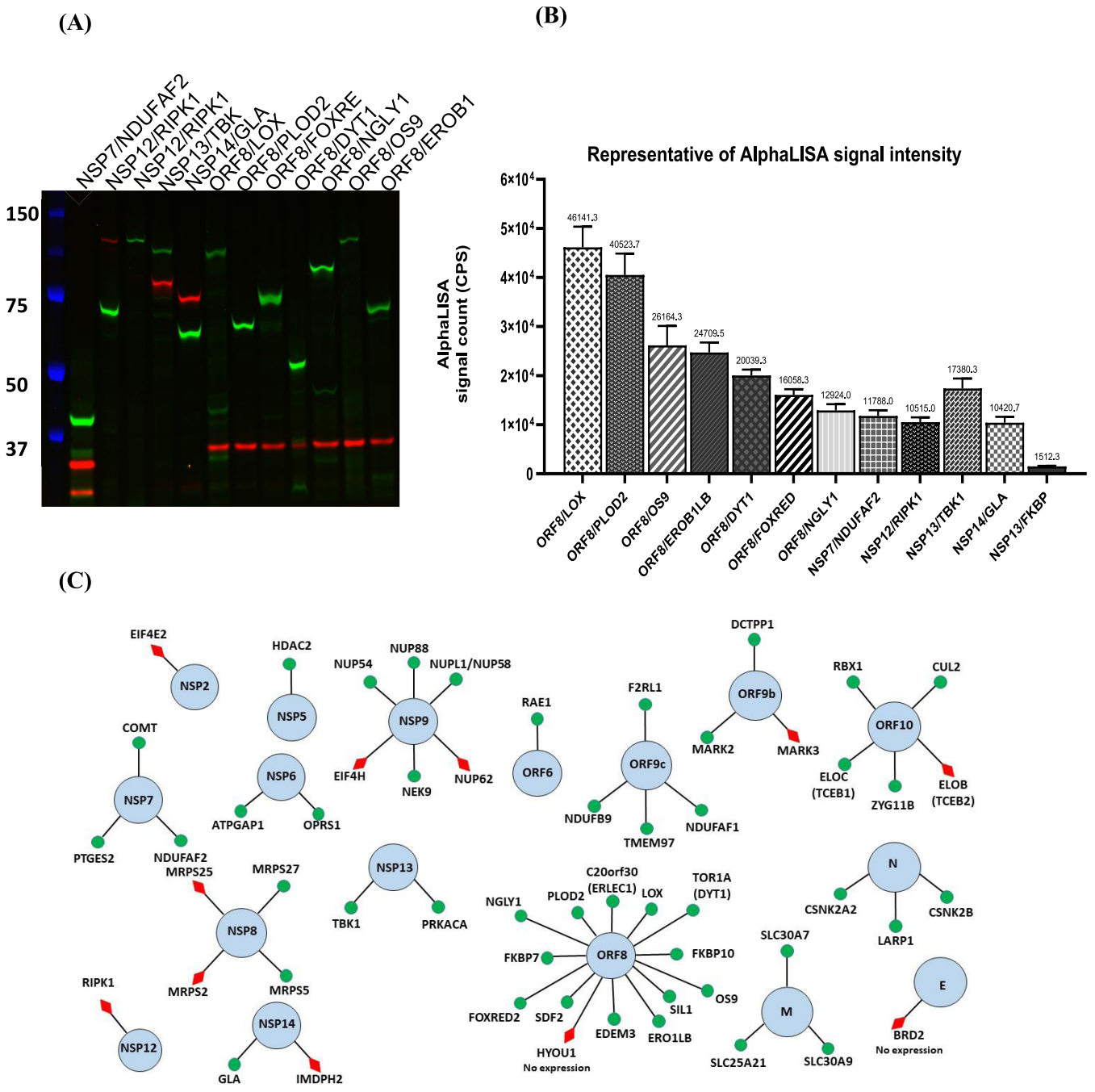

Figure 2. Interaction analysis of SARS-CoV-2 and human proteins produced in the LTE expression system. (A) Representative image of the SDS-PAGE gel loaded with LTE translation reactions of co-expressed human druggable proteins and SARS-CoV-2 polypeptides. Human proteins were tagged with eGFP at the N-terminus, while the viral proteins were tagged with mCherry at the C-terminus. The protein bands were visualized by fluorescence scanning of the unstained gels; viral proteins: NSP7, NSP12, NSP13, NSP14, and ORF8; human proteins: NDUFAF2, RIPK1, TBK1, GLA, PLOD2, LOX, FOXRED, DYT1, NGLY1, OS9, and EROB1. (B) Plot of the representative AlphaLISA signal intensities obtained for human-viral protein pairs from panel (A). The interaction signals are derived from three experimental repeats (mean ± SD) for 11 protein interacting partners. The FK506-binding protein (FKBP) was used as a negative control of the assay. (C) Graphic summary of the human/SARS-CoV-2 protein−protein interaction analysis results. The confirmed interactions are shown as green circles, whereas interactions that could not be identified using this assay are depicted as red diamonds.

subset, HYOU1 was not produced at the detectable level and the expression yield of BRD2 was low (Figure S1B). Therefore, these two proteins were excluded from further interaction analysis.

To analyze protein−protein interactions, the human proteins tagged with eGFP at the N-terminus were co-expressed in LTE with the putative viral interacting partners tagged with mCherry at the C-terminus (Figure 2A). The lysate expressing such protein pairs was subjected to AlphaLISA analysis as described above. The AlphaLISA signal intensities detected in interactions ranged between 1.05×10^4 and 5.3×10^4 CPS (Figure 2B and Table S3).

The analysis of 54 tested putative protein−protein interactions led to the detection of 45 human-viral interacting

https://doi.org/10.1021/acsomega.3c01625
ACS Omega 2023, 8, 25009−25019

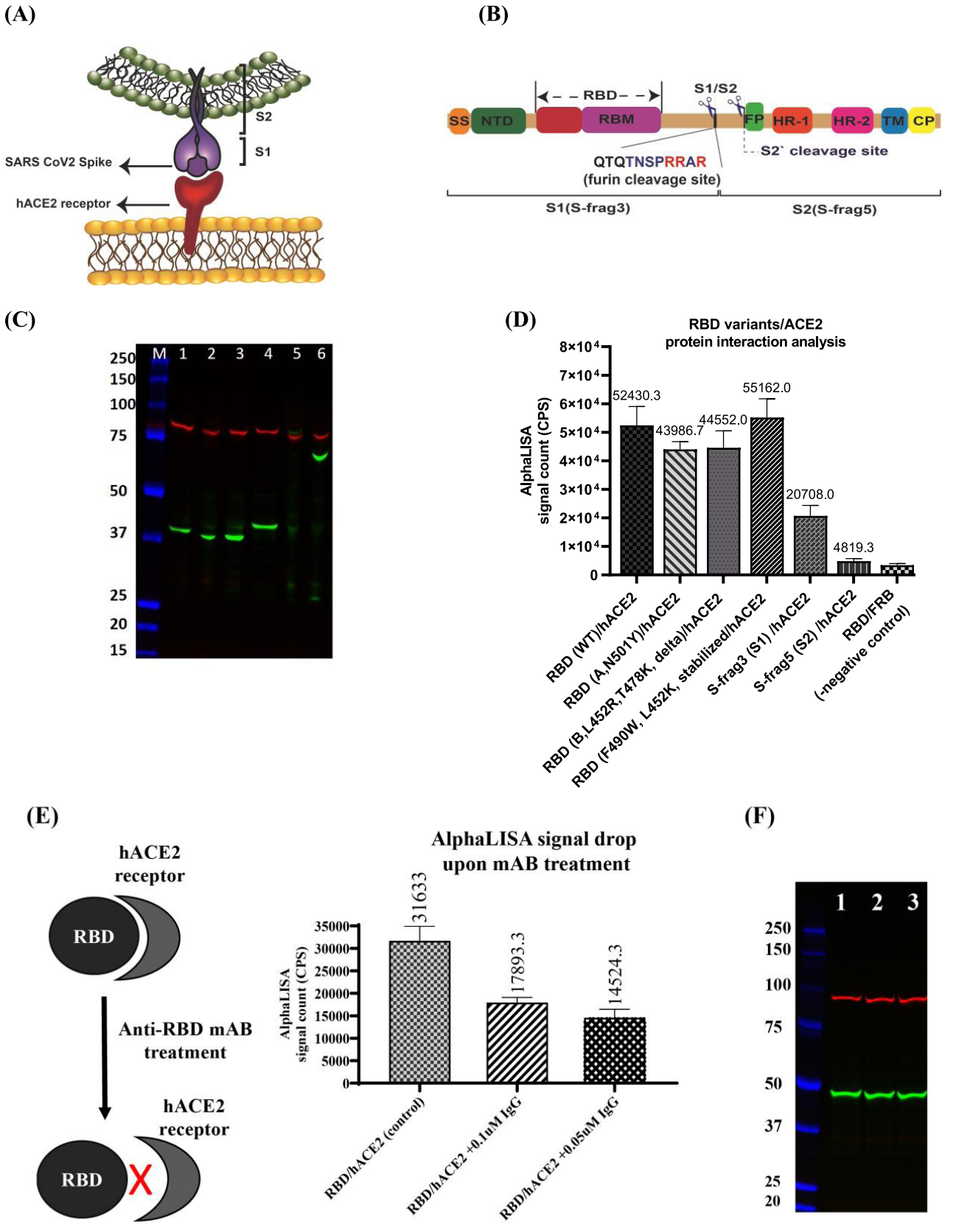

Figure 3. (A) Schematic representation of the SARS-CoV-2 spike protein interacting with the hACE2 receptor. (B) Schematic domain organization of the spike protein gene structure. S1 (S-frag3), receptor-binding subunit; S2 (S-frag5), membrane fusion subunit; TM, transmembrane anchor; CP, cytoplasmic domain; NTD, N-terminal domain; FP, fusion peptide, HR1 heptad repeat 1, and HR2, heptad repeat 2 are structural units in the coronavirus. (C) SDS-PAGE gel image of RBD variants and spike domains of SARS-CoV-2 co-expressed with the hACE2 receptor in the LTE system; RBD proteins are tagged with eGFP at the N-terminus and hACE2 receptor is fused with mCherry at the C-terminus. Lane 1: RBD (WT), lane 2: RBD (A), lane 3: RBD (B), lane 4: RBD (stabilized), lane 5: S-frag3, and lane 6: S-frag5. The S-frag3 protein sequence contains the N-

https://doi.org/10.1021/acsomega.3c01625
ACS Omega 2023, 8, 25009−25019

Figure 3. continued

terminal fragment after the furin cleavage, whereas S-frag5 includes the C-terminal ectodomain after the furin cleavage site. (D) AlphaLISA signals obtained from *in vitro* protein−protein interaction analysis of RBD protein variants with the hACE2 receptor. The interaction of hACE2 with all tested RBD variants and the S1 subunit produced AlphaLISA positive signals (over 2×10^4 CPS vs. 3.2×10^3 CPS for RBD/FRB as a negative control), confirming the direct interaction of RBD with the hACE2 receptor. The FRB protein was used as a negative control of the assay. (E) Inhibitory effect of the anti-RBD antibody on RBD binding to the hACE2 receptor; the LTE reaction expressing RBD/hACE2 was treated with 100 and 50 nM anti-RBD antibodies, resulting in a 50% drop in the AlphaLISA signal, confirming the inhibition of RBD to the receptor. (F) Adding the mAB at the start of the LTE expression reaction did not affect or reduce the protein expression level. The green band shows RBD and the mCherry band is hACE2; lane 1: control (untreated reaction) and lanes 2 and 3: treated with 100 and 50 nM stabilized anti-RBD antibodies.

pairs, with 9 human-viral protein pairs displaying no detectable interactions. The resulting interaction map is presented in Figure 2C. These protein pairs were reanalyzed by relocating the fluorescent domain to the other termini in order to rule out the tag position effect on protein−protein interactions.[26] Performing the latter test did not change the assay's results, and therefore, those protein pairs were classified as non-interacting with a caveat that additional factors might have led to false negative signals. First, the LTE cell-free system produces approximately 70% of human proteins in a folded and monodispersed form,[21] and therefore, some of the proteins in our set might not be functional. Second, *in vivo* post-translational modifications may modulate host protein interactions with viral ORFs. Many of such modifications are expected to be inefficient or absent in LTE. Finally, in some of the interactions, additional proteins might be required to form higher-order complexes that contribute to the overall affinity of the interaction. Therefore, binary interactions may have affinities that are below the detection threshold of our assay. This could be the reason why we were not able to identify the interaction between EIF4E2 and NSP2, as the GIGYF2 protein is required for protein complex formation.[9,39]

Interaction Analysis of SARS-CoV-2 Spike and RBD Protein Variants with the hACE2 Receptor. The importance of the hACE2/S protein and hACE2/RBD interactions in host cell entry and initiation of infection motivated us to test whether these could be reconstituted using the developed assay. The S protein is a crucial component of SARS-CoV-2 host infection as it mediates viral entry into cells. It consists of 1273 amino acid residues, cleaved with furin protease at the polybasic insertion site into parts S1 and S2.[40] The RBD in the S1 subunit interacts with the hACE2 receptor, which is the primary cellular receptor of the virus and is required for the virus internalization. The S2 subunit mediates the membrane fusion for virus entry to the host (Figure 3A,B).[41,42] In this study, we used the S1 (S-frag3) sequence that covers the N-terminal domain of spike (NTD), RBD, and the furin cleavage site (Table S1). The S2 subunit (S-frag5) encodes the C-terminal ectodomain of the S protein without the furin cleavage site.[43] As expected, the LTE-expressed S1 subunit and hACE2 receptor displayed a clear interaction (22×10^3 CPS) that, presumably, occurred via the receptor-binding motif (RBM), whereas no hACE2 interaction was detected with the S2 subunit (4.2×10^3 CPS) (Figure 3D).

Over the years of the pandemic, the SARS-CoV-2 virus has undergone substantial changes and generated a number of variants such as α (B.1.1.7), β (B.1.351), γ (P.1), Mu (B.1.621), and more recently, Omicron (B.1.1.529) that share an N501Y mutation at the RBD of the S protein.[44,45] The N501Y substitution is the only mutation on the interface between the RBD of B.1.1.7 and hACE2.[46] This mutation enhances the infectivity and transmission of the virus.[47] The Delta variant (B.1.617.20) lacks the N501Y mutation but bears double mutations (L452R, T478K) in the RBD, leading to increased infectivity and immune response evasion.[48,49] We have tested the expression and interactions of these mutations in our system. A positive AlphaLISA signal was obtained for all RBD variants ranging between 44×10^3 and 55×10^3 CPS, which were at least 10 times greater than the negative control signals (4.2×10^3 CPS). The hACE2 interaction with a stabilized RBD variant designed by Dalvie et al.[50] was also analyzed in the LTE system, and the observed AlphaLISA signal of 55.2×10^3 CPS was comparable to the other RBD mutants (Figure 3C,D). These results demonstrate that all RBD variants were produced in a functional state, suggesting that this platform can be used as a facile approach toward prototyping mutated proteins.

Next, we decided to evaluate the potential applicability of the developed interaction assay for testing neutralizing antibody candidates. The inhibitory effect of the anti-RBD monoclonal antibody (mAB) on the RBD/hACE2 interaction was examined by adding the mAB to a final concentration of 0.1 and 0.5 μM to the *in vitro* expression reaction at the start of the protein production. The expressed reactions were subjected to the AlphaLISA assay to investigate the interaction signal change compared to the untreated reaction. The AlphaLISA signal decreased from $\sim 32 \times 10^3$ to $\sim 18 \times 10^3$ and $\sim 14 \times 10^3$ CPS at the respective antibody concentrations, confirming the ability of the mAB to disrupt the RBD−hACE2 interaction (Figure 3E,F).

DISCUSSION

Emerging pathogens with pandemic potential pose a major challenge to the technologies used for their analysis, as an understanding of pathogenesis needs to be achieved rapidly. In particular, the complex protein−protein interaction networks that underlie host−pathogen interactions cannot be easily reconstituted and analyzed. While proteomic analysis can identify putative interacting partners, as with any other high-throughput method, it requires extensive experimental validation. In this study, we employed methods of expressed *in vitro* proteomics to analyze intraviral and host−virus protein−protein interaction networks of the SARS-CoV-2 virus. In this study, we demonstrated the rapid expression of viral and human proteins in the eukaryotic LTE cell-free system, followed by protein−protein interaction analysis using the bead proximity AlphaLISA assay. The developed workflow is multiplexable, rapid, and rate-limited only by the speed of template generation. Interaction analysis demonstrated that 80% of protein−protein interactions between viral and human proteins identified by mass spectrometry could be reconstituted in this system.

We propose that the presented interaction screening approach provides a platform for detailed analysis of individual

https://doi.org/10.1021/acsomega.3c01625
ACS Omega 2023, 8, 25009−25019

protein−protein interactions that can be utilized as a screening platform for lead therapeutic compounds. For example, the cost of producing 100 protein pairs in LTE and performing its protein−protein interaction analysis using the described method is estimated to be around 2600 USD. This calculation is based on the cost of reagents and labor cost but excludes the cost of DNA template sourcing and cloning, which varies widely depending on its origin. The protein−protein interaction analysis would take between 10 and 20 days, depending on the time required to optimize protein pair co-expression. During the revision, we were asked by the referee to provide the cost estimation for screening 1,000,000 compounds against one interacting protein pair. The cost of protein production would be in the range of 30,000 USD, assuming the consumption of 0.75 μL of protein-expressing LTE lysate per assay and lysate cost of 40 USD/mL. With approximate cost estimations of beads and plastic ware, the cost of interaction assay is close to one USD/sample. Using automated liquid handling for compound screening, the assay can be performed within 10−15 days. As a casing example, we demonstrated that anti-RBD antibodies can inhibit the interaction of *in vitro*-produced RBD with its cellular target, the hACE2 receptor. Therefore, the developed platform allows rapid mapping of the host−virus interaction and simultaneous development of assays for identification of their modulators.

MATERIALS AND METHODS

Construction of Expression Plasmids. The DNA sequences of SARS-CoV-2 were sourced from the isolate of 2019-nCoV/USA-WA1/2020 (accession number MN985325) and based on the published annotation of the genome sequence of SARS-CoV-2.[9] From 30 viral genes, 24 genes were synthesized by Gene Universal Inc. or GenScript and inserted into pCellFree_G06, pmCell-free_KA1, and/or pmCell-free_KA3 gateway destination vectors, respectively, available in Addgene, Plasmid # 67140: https://www.addgene.org/67140/; Plasmid #145369: https://www.addgene.org/145369/; Plasmid #169408:https://www.addgene.org/169408/. The pmCell-free_KA1 backbone contains a T7 promoter, CMV enhancer, and chicken β-actin promoter and encodes 8xHis and eGFP tags at the 5′ end of the open reading frame,[26] whereas pCellFree_G06 contains a T7 promoter and encodes 8xHis and mCherry tags at the 3′ end of the gene of interest insertion site.[51] The NSP11 gene was excluded from the plasmid construction as it is a small 13 amino acid disordered peptide.[52]

Six viral genes were purchased from Addgene in Gateway donor vectors (as deposited by Roth and Taipale).[43] The genes were transferred to the aforementioned destination vectors using the standard Gateway cloning strategy. The Addgene codes of purchased plasmids are as follows: NSP3, Plasmid #149306; NSP12, Plasmid #149314; NSP15, Plasmid #149317; S, Plasmid #152988; S-frag3, Plasmid #153175; S-frag5, Plasmid #153177. All cell-free viral expression vectors with N-terminal eGFP were deposited in Addgene. The Addgene codes of deposited plasmids are provided in Supporting Table S1.

Sequences coding the genes for human SARS-CoV-2 interacting proteins were sourced from the human ORFeome V2 version maintained in the DNASU plasmid repository (Arizona State University). The ORFs were cloned into pmCell-free_KA1 and pCellFree_G06 gateway destination vectors, and cloning was carried out by the DNASU plasmid repository (Table S2).

The coding sequence of the N-terminal peptidase domain of human angiotensin-converting enzyme 2 (hACE2; residues Ser19−Asp615) was cloned into pmCell-free_KA3 (https://www.addgene.org/169408/). The pmCell-free_KA3 contains a T7 promoter, CMV enhancer, and chicken β-actin promoter in addition to mCherry and 6xHis tag at the C-terminal region of open reading frames.

The gene sequences of SARS-CoV-2 RBD variants including wild-type (WT) RBD, RBD (N501Y, mutual mutation in α, β, and γ), RBD (L452R, T478K, delta variant), and engineered RBD (L452K-F490W)[50] were inserted into the pmCell-free_KA1 vector.

All synthesized plasmids DNA were amplified and isolated by the NucleoBond Xtra Midi kit (Macherey Nagel; Germany). The gene sequences are provided in Table S1.

Expression of SARS-CoV-2 Proteins in the Cell-Free LTE System. All 28 SARS-CoV-2 genes were expressed in cell-free LTE individually. The NSP11 gene was excluded from the plasmid construction as it is a small 13 amino acid disordered peptide.[52] The detailed procedure for the *L. tarentolae* translation extract and the feeding solution for protein expression were described previously.[23] The expression reaction was performed in 384-well Proxiplates (PerkinElmer; Australia) in 10 μL volume containing DNA templates (10−25 nM, depending on the vector size), LTE extract (5 μL), feeding solution (5×, 2 μL), and ultrapure water (ThermoFisher; Australia). The reactions were incubated for 3 and 5 h (eGFP and mCherry fusions, respectively) at 25 °C. The expressed proteins were detected by measuring eGFP and mCherry fluorescence signals using a Tecan Spark multimode microplate reader (Tecan Australia Pty Ltd.). The wavelength and bandwidth parameters for both fluorophores to capture the optimum signals were set as follows: eGFP fluorophore: excitation and emission wavelength: 486 and 516 nm, respectively, and bandwidth: 5 nm; mCherry fluorophore: excitation and emission wavelength: 560 and 620 nm, respectively, and bandwidth: 5 nm. The protein quantity was estimated fluorometrically using a standard curve of pure eGFP produced in-house.

To analyze the quality and integrity of eGFP and mCherry fused proteins, the LTE reactions were mixed with 1:1 v/v of 2× NuPAGE sample buffer (ThermoFisher, Australia) and resolved on a Bolt 4−12% Bis-Tris protein gel (ThermoFisher, Australia). The proteins were detected by scanning the gel using the ChemiDoc MP System (Bio-Rad, Australia). To quantify eGFP fused proteins, 10 μL of serially diluted pure eGFP ranging from 50 to 10 μg/mL was loaded on the SDS-PAGE gel along with fusion proteins, and the resolved protein bands were quantified using Image Lab software (Version 6.1, Bio-Rad).

***In Vivo* Expression of Viral Proteins in HEK293T Cells.** HEK293T cells (Sourced from ATCC, CRL-3216) were used for transient transfection of SARS-CoV-2 proteins. Cells were grown in 75 cm^2 culture flasks containing Dulbecco's modified Eagle's medium (DMEM) supplemented with 10% fetal bovine serum (FBS), 1% MEM nonessential amino acid, 1% L-glutamine, 100 units per mL penicillin, and 100 units per mL streptomycin (all solutions were purchased from Gibco, Thermofisher: Australia) and maintained at 37 °C with a 5% CO_2 atmosphere.

https://doi.org/10.1021/acsomega.3c01625
ACS Omega 2023, 8, 25009−25019

For transient transfection, HEK293T cells were seeded at 5 × 10^4 in Corning Costar 48 well TC-treated plates (Corning, Germany) in 200 μL of supplemented DMEM without antibiotics and incubated overnight at 37 °C and 5% CO_2. On the transfection day, pmCell-free plasmids (600 ng per well) were diluted in 200 μL of Opti-MEM reduced-serum medium (Gibco, Thermofisher: Australia) mixed with the Lipofectamine 2000 reagent (Life Technologies, AUS) in a 1:1.5 ratio of DNA/lipofectamine according to the manufacturer's protocol. The mixture was incubated at RT for 20 min. The growth media was removed from the plate and replaced with 150 μL of prewarmed supplemented DMEM without antibiotics, followed by dropwise addition of the DNA/lipofectamine complex. Following a 6 h incubation of the cells with the DNA complex at 37 °C, the growth media was removed and replaced by fresh 10% FBS/DMEM medium (w/o antibiotics), and the culture plate was incubated at 37 °C overnight. The transfected cells were imaged 24 h post-transfection using a Nikon Eclipse TS2 inverted microscope (Scope Scientific, AUS) equipped with fluorescent filters and a cooled color camera.

LTE Co-Expression of Human Proteins and the Viral Interacting Partners. The human and viral protein pairs were co-expressed in the LTE cell-free expression system. The DNA templates for N-terminal-GFP (8−12 nM)- and C-terminal-Cherry (10−15 nM)-tagged proteins were added concomitantly to the LTE reaction mixture, and the samples were incubated for 5 h at 25 °C for expression. The expression of proteins was performed using 384-well Proxiplate in 10 μL volume. The reaction was monitored with the Tecan Spark multimode microplate reader, and the quality of the co-expressed proteins was evaluated by separating the protein bands on the SDS-PAGE gel as described before. The co-expressed protein pairs were subjected to the AlphaLISA assay directly (without purification and extra treatment) for interaction analysis.

Protein−Protein Interaction Setup (AlphaLISA Assay). AlphaLISA assays were performed in Optiplate-384 plus plates using Anti-GFP AlphaLISA Acceptor (AL133C, PerkinElmer, AUS) and Streptavidin Donor beads (AL125C, PerkinElmer, AUS). α beads were prepared according to the protocol provided by the manufacturer.[53] Briefly, the acceptor and donor bead stocks (5 mg/mL) were diluted to 100 μg/mL (5×) in AlphaLISA assay buffer (Buffer A: 25 mM HEPES, 50 mM NaCl, 0.1% BSA and 0.01% Nonidet P-40; pH: 7.5). The biotinylated mCherry nanobody (prepared in-house)[23] diluted in buffer A (final concentration of 4 nM) was added into microplate wells, followed by the addition 15 μL of LTE lysate diluted 1:20 with assay buffer and containing putative interacting proteins (diluted 20× in AlphaLISA assay buffer) and 5 μL of the acceptor beads (5×). The samples were incubated for 30 min at room temperature. Subsequently, 5 μL of donor beads (5×) were added to samples under low light conditions and incubated for 30 min at room temperature. For all experiments, samples were prepared in triplicate and the assay was repeated 2 times. The AlphaLISA signal was detected with the Tecan Spark multimode microplate reader using the following settings: mode: AlphaLISA, excitation time: 130 ms, and integration time: 300 ms. In α screen experiments, the FKBP-rapamycin binding (FRB) protein was used as a negative control.

RBD−hACE2 Interaction Assay. The gene sequences of SARS-CoV-2 RBD (residues Arg319−Phe541) and the N-terminal peptidase domain of hACE2 (residues Ser19−Asp615)[38] were inserted in pmCell-free_KA1 and pCell-Free_G06, respectively. eGFP-RBD (7 nM, 30 ng/μL) and hACE2-mCherry (12 nM, 40 ng/μL) plasmids were added to 7 μL of the supplemented LTE reaction mixture and the mixture was topped up with ultrapure water to 10 μL. The reaction was incubated for 5 h at 25 °C. The AlphaLISA assay was performed as described earlier.

For analysis of the anti-RBD antibody-mediated inhibition of the RBD/hACE2 interaction, the mAB purchased from Sanyou Biopharmaceuticals (#AHA004) was diluted with PBS to the final concentrations of 1.0 and 0.5 μM stock. Following the preparation of the 10 μL LTE reaction for co-expression of eGFP-RBD and hACE2-mCherry, 1 μL of the mAB stock solutions were added to the reactions at the start of expression. After 5 h, the samples were diluted 20× with AlphaLISA assay buffer and subjected to the AlphaLISA assay.

■ ASSOCIATED CONTENT

Supporting Information

The Supporting Information is available free of charge at https://pubs.acs.org/doi/10.1021/acsomega.3c01625.

SDS-PAGE gel image of CFPS expressed proteins; protein quantification; HEK293 cell images expressing viral proteins, and AlphaLISA signal intensities of intraviral PPIs (PDF)

Human and viral gene sequences table and AlphaLISA signal intensities of human-viral PPIs (XLSX)

■ AUTHOR INFORMATION

Corresponding Author

Kirill Alexandrov − *CSIRO-QUT Synthetic Biology Alliance, ARC Centre of Excellence in Synthetic Biology, Centre for Agriculture and the Bioeconomy, Centre for Genomics and Personalised Health, School of Biology and Environmental Science, Queensland University of Technology, Brisbane, QLD 4001, Australia;* orcid.org/0000-0002-0957-6511; Email: kirill.alexandrov@qut.edu.au

Authors

Shayli Varasteh Moradi − *CSIRO-QUT Synthetic Biology Alliance, ARC Centre of Excellence in Synthetic Biology, Centre for Agriculture and the Bioeconomy, Centre for Genomics and Personalised Health, School of Biology and Environmental Science, Queensland University of Technology, Brisbane, QLD 4001, Australia*

Yue Wu − *CSIRO-QUT Synthetic Biology Alliance, ARC Centre of Excellence in Synthetic Biology, Centre for Agriculture and the Bioeconomy, Centre for Genomics and Personalised Health, School of Biology and Environmental Science, Queensland University of Technology, Brisbane, QLD 4001, Australia;* Present Address: Cold Spring Harbor Laboratory, Cold Spring Harbor, New York, New York 11724, USA

Patricia Walden − *CSIRO-QUT Synthetic Biology Alliance, ARC Centre of Excellence in Synthetic Biology, Centre for Agriculture and the Bioeconomy, Centre for Genomics and Personalised Health, School of Biology and Environmental Science, Queensland University of Technology, Brisbane, QLD 4001, Australia*

Zhenling Cui − *CSIRO-QUT Synthetic Biology Alliance, ARC Centre of Excellence in Synthetic Biology, Centre for*

https://doi.org/10.1021/acsomega.3c01625
ACS Omega 2023, 8, 25009−25019

Agriculture and the Bioeconomy, Centre for Genomics and Personalised Health, School of Biology and Environmental Science, Queensland University of Technology, Brisbane, QLD 4001, Australia

Wayne A. Johnston − *CSIRO-QUT Synthetic Biology Alliance, ARC Centre of Excellence in Synthetic Biology, Centre for Agriculture and the Bioeconomy, Centre for Genomics and Personalised Health, School of Biology and Environmental Science, Queensland University of Technology, Brisbane, QLD 4001, Australia*

Dmitri Petrov − *Department of Biology, Stanford University, Stanford, California 94305-5020, United States*

Complete contact information is available at: https://pubs.acs.org/10.1021/acsomega.3c01625

Author Contributions

S.V.M.—designed experiments, performed experiments, analyzed data, and wrote the manuscript, Y.W. and Z.C.—performed experiments and analyzed data, W.A.J.—performed experiments and analyzed data, P.W.—performed experiments, D.P.—designed experiments, analyzed data, and wrote the manuscript, and K.A.—designed experiments, analyzed data, and wrote the manuscript.

Notes

The authors declare no competing financial interest.

In late 2019, the emergence of the highly infectious virus called severe acute respiratory syndrome coronavirus-2 (SARS-CoV-2) caused the coronavirus disease (COVID-19) pandemic that unfolded into a global health crisis. Mapping the host−pathogen protein−protein interaction network is a key to understanding the mechanisms of viral biogenesis and its subsequent evolution. Using LTE cell-free protein expression in combination with AlphaLISA protein−protein interaction analysis, we tested SARS-CoV-2 17 intraviral and 54 host-viral protein−protein interactions. This approach resulted in the confirmation of 12 putative intraviral homo- and heterodimeric interactions as well as 45 human-viral protein interactions. In addition, we performed a detailed analysis of the SARS-CoV-2 RBD's interaction with the human hACE2 receptor and demonstrated the suitability of this assay for inhibitory antibody screening. We performed protein−protein interaction analysis on both SARS-CoV-2 intraviral and host-viral interacting proteins. By employing this all-*in vitro* approach, the direct protein interaction of 17 intraviral and 54 human-viral protein pairs was investigated, allowing confirmation of 12 intraviral homo- and heteroprotein dimers and 45 human-viral protein partners. In addition, the potential application of this platform for antibody screening against the SARS-CoV-2 RBD was demonstrated.

■ ACKNOWLEDGMENTS

This project has been funded in part by the ARC Centre of Excellence in Synthetic Biology CE200100029 to K.A. The authors acknowledge the support of Stanford RISE COVID-19 Crisis Response Faculty Seed Grant Program to D.P. We thank PerkinElmer Inc. for providing free-of-charge AlphaLISA beads used in this study.

■ REFERENCES

(1) WHO. WHO Director-General's opening remarks at the media briefing on COVID-19-11 March 2020. https://www.who.int/director-general/speeches/detail/who-director-general-s-opening-remarks-at-the-media-briefing-on-covid-19---11-march-2020.

(2) Kim, D.; Lee, J.-Y.; Yang, J.-S.; Kim, J. W.; Kim, V. N.; Chang, H. The Architecture of SARS-CoV-2 Transcriptome. *Cell* **2020**, *181*, 914−921.e10.

(3) Zhou, P.; Yang, X.-L.; Wang, X.-G.; Hu, B.; Zhang, L.; Zhang, W.; Si, H.-R.; Zhu, Y.; Li, B.; Huang, C.-L.; et al. A pneumonia outbreak associated with a new coronavirus of probable bat origin. *Nature* **2020**, *579*, 270−273.

(4) Romano, M.; Ruggiero, A.; Squeglia, F.; Maga, G.; Berisio, R. J. C. A structural view of SARS-CoV-2 RNA replication machinery: RNA synthesis, proofreading and final capping. *Cells* **2020**, *9*, No. 1267.

(5) V'kovski, P.; Kratzel, A.; Steiner, S.; Stalder, H.; Thiel, V. Coronavirus biology and replication: implications for SARS-CoV-2. *Nat. Rev. Microbiol.* **2021**, *19*, 155−170.

(6) Chan, J. F.-W.; Kok, K.-H.; Zhu, Z.; Chu, H.; To, K. K.-W.; Yuan, S.; Yuen, K.-Y. Genomic characterization of the 2019 novel human-pathogenic coronavirus isolated from a patient with atypical pneumonia after visiting Wuhan. *Emerging Microbes Infect.* **2020**, *9*, 221−236.

(7) Newman, J. A.; Douangamath, A.; Yadzani, S.; Yosaatmadja, Y.; Aimon, A.; Brandão-Neto, J.; Dunnett, L.; Gorrie-stone, T.; Skyner, R.; Fearon, D.; Schapira, M.; von Delft, F.; Gileadi, O. Structure, mechanism and crystallographic fragment screening of the SARS-CoV-2 NSP13 helicase. *Nat. Commun.* **2021**, *12*, No. 4848.

(8) Michel, C. J.; Mayer, C.; Poch, O.; Thompson, J. D. Characterization of accessory genes in coronavirus genomes. *Virol. J.* **2020**, *17*, No. 131.

(9) Gordon, D. E.; Jang, G. M.; Bouhaddou, M.; Xu, J.; Obernier, K.; White, K. M.; O'Meara, M. J.; Rezelj, V. V.; Guo, J. Z.; Swaney, D. L.; Tummino, T. A.; Hüttenhain, R.; Kaake, R. M.; Richards, A. L.; Tutuncuoglu, B.; Foussard, H.; Batra, J.; Haas, K.; Modak, M.; Kim, M.; Haas, P.; Polacco, B. J.; Braberg, H.; Fabius, J. M.; Eckhardt, M.; Soucheray, M.; Bennett, M. J.; Cakir, M.; McGregor, M. J.; Li, Q.; Meyer, B.; Roesch, F.; Vallet, T.; Mac Kain, A.; Miorin, L.; Moreno, E.; Naing, Z. Z. C.; Zhou, Y.; Peng, S.; Shi, Y.; Zhang, Z.; Shen, W.; Kirby, I. T.; Melnyk, J. E.; Chorba, J. S.; Lou, K.; Dai, S. A.; Barrio-Hernandez, I.; Memon, D.; Hernandez-Armenta, C.; Lyu, J.; Mathy, C. J. P.; Perica, T.; Pilla, K. B.; Ganesan, S. J.; Saltzberg, D. J.; Rakesh, R.; Liu, X.; Rosenthal, S. B.; Calviello, L.; Venkataramanan, S.; Liboy-Lugo, J.; Lin, Y.; Huang, X.-P.; Liu, Y.; Wankowicz, S. A.; Bohn, M.; Safari, M.; Ugur, F. S.; Koh, C.; Savar, N. S.; Tran, Q. D.; Shengjuler, D.; Fletcher, S. J.; O'Neal, M. C.; Cai, Y.; Chang, J. C. J.; Broadhurst, D. J.; Klippsten, S.; Sharp, P. P.; Wenzell, N. A.; Kuzuoglu-Ozturk, D.; Wang, H.-Y.; Trenker, R.; Young, J. M.; Cavero, D. A.; Hiatt, J.; Roth, T. L.; Rathore, U.; Subramanian, A.; Noack, J.; Hubert, M.; Stroud, R. M.; Frankel, A. D.; Rosenberg, O. S.; Verba, K. A.; Agard, D. A.; Ott, M.; Emerman, M.; Jura, N.; von Zastrow, M.; Verdin, E.; Ashworth, A.; Schwartz, O.; d'Enfert, C.; Mukherjee, S.; Jacobson, M.; Malik, H. S.; Fujimori, D. G.; Ideker, T.; Craik, C. S.; Floor, S. N.; Fraser, J. S.; Gross, J. D.; Sali, A.; Roth, B. L.; Ruggero, D.; Taunton, J.; Kortemme, T.; Beltrao, P.; Vignuzzi, M.; García-Sastre, A.; Shokat, K. M.; Shoichet, B. K.; Krogan, N. J. A SARS-CoV-2 protein interaction map reveals targets for drug repurposing. *Nature* **2020**, *583*, 459−468.

(10) Stukalov, A.; Girault, V.; Grass, V.; Karayel, O.; Bergant, V.; Urban, C.; Haas, D. A.; Huang, Y.; Oubraham, L.; Wang, A.; Hamad, M. S.; Piras, A.; Hansen, F. M.; Tanzer, M. C.; Paron, I.; Zinzula, L.; Engleitner, T.; Reinecke, M.; Lavacca, T. M.; Ehmann, R.; Wölfel, R.; Jores, J.; Kuster, B.; Protzer, U.; Rad, R.; Ziebuhr, J.; Thiel, V.; Scaturro, P.; Mann, M.; Pichlmair, A. Multilevel proteomics reveals host perturbations by SARS-CoV-2 and SARS-CoV. *Nature* **2021**, *594*, 246−252.

(11) Gordon, D. E.; Hiatt, J.; Bouhaddou, M.; Rezelj, V. V.; Ulferts, S.; Braberg, H.; Jureka, A. S.; Obernier, K.; Guo, J. Z.; Batra, J.; Kaake, R. M.; Weckstein, A. R.; Owens, T. W.; Gupta, M.; Pourmal, S.; Titus, E. W.; Cakir, M.; Soucheray, M.; McGregor, M.; Cakir, Z.; Jang, G.; O'Meara, M. J.; Tummino, T. A.; Zhang, Z.; Foussard, H.; Rojc, A.; Zhou, Y.; Kuchenov, D.; Hüttenhain, R.; Xu, J.; Eckhardt, M.;

Swaney, D. L.; Fabius, J. M.; Ummadi, M.; Tutuncuoglu, B.; Rathore, U.; Modak, M.; Haas, P.; Haas, K. M.; Naing, Z. Z. C.; Pulido, E. H.; Shi, Y.; Barrio-Hernandez, I.; Memon, D.; Petsalaki, E.; Dunham, A.; Marrero, M. C.; Burke, D.; Koh, C.; Vallet, T.; Silvas, J. A.; Azumaya, C. M.; Billesbølle, C.; Brilot, A. F.; Campbell, M. G.; Diallo, A.; Dickinson, M. S.; Diwanji, D.; Herrera, N.; Hoppe, N.; Kratochvil, H. T.; Liu, Y.; Merz, G. E.; Moritz, M.; Nguyen, H. C.; Nowotny, C.; Puchades, C.; Rizo, A. N.; Schulze-Gahmen, U.; Smith, A. M.; Sun, M.; Young, I. D.; Zhao, J.; Asarnow, D.; Biel, J.; Bowen, A.; Braxton, J. R.; Chen, J.; Chio, C. M.; Chio, U. S.; Deshpande, I.; Doan, L.; Faust, B.; Flores, S.; Jin, M.; Kim, K.; Lam, V. L.; Li, F.; Li, J.; Li, Y.-L.; Li, Y.; Liu, X.; Lo, M.; Lopez, K. E.; Melo, A. A.; Moss, F. R.; Nguyen, P.; Paulino, J.; Pawar, K. I.; Peters, J. K.; Pospiech, T. H.; Safari, M.; Sangwan, S.; Schaefer, K.; Thomas, P. V.; Thwin, A. C.; Trenker, R.; Tse, E.; Tsui, T. K. M.; Wang, F.; Whitis, N.; Yu, Z.; Zhang, K.; Zhang, Y.; Zhou, F.; Saltzberg, D.; Consortium12†, Q. S. B.; Hodder, A. J.; Shun-Shion, A. S.; Williams, D. M.; White, K. M.; Rosales, R.; Kehrer, T.; Miorin, L.; Moreno, E.; Patel, A. H.; Rihn, S.; Khalid, M. M.; Vallejo-Gracia, A.; Fozouni, P.; Simoneau, C. R.; Roth, T. L.; Wu, D.; Karim, M. A.; Ghoussaini, M.; Dunham, I.; Berardi, F.; Weigang, S.; Chazal, M.; Park, J.; Logue, J.; McGrath, M.; Weston, S.; Haupt, R.; Hastie, C. J.; Elliott, M.; Brown, F.; Burness, K. A.; Reid, E.; Dorward, M.; Johnson, C.; Wilkinson, S. G.; Geyer, A.; Giesel, D. M.; Baillie, C.; Raggett, S.; Leech, H.; Toth, R.; Goodman, N.; Keough, K. C.; Lind, A. L.; Zoonomia, C.; Klesh, R. J.; Hemphill, K. R.; Carlson-Stevermer, J.; Oki, J.; Holden, K.; Maures, T.; Pollard, K. S.; Sali, A.; Agard, D. A.; Cheng, Y.; Fraser, J. S.; Frost, A.; Jura, N.; Kortemme, T.; Manglik, A.; Southworth, D. R.; Stroud, R. M.; Alessi, D. R.; Davies, P.; Frieman, M. B.; Ideker, T.; Abate, C.; Jouvenet, N.; Kochs, G.; Shoichet, B.; Ott, M.; Palmarini, M.; Shokat, K. M.; García-Sastre, A.; Rassen, J. A.; Grosse, R.; Rosenberg, O. S.; Verba, K. A.; Basler, C. F.; Vignuzzi, M.; Peden, A. A.; Beltrao, P.; Krogan, N. J.; Owens, T. W.; Gupta, M.; Pourmal, S.; Titus, E. W.; Azumaya, C. M.; Billesbølle, C.; Brilot, A. F.; Campbell, M. G.; Diallo, A.; Dickinson, M. S.; Diwanji, D.; Herrera, N.; Hoppe, N.; Kratochvil, H. T.; Liu, Y.; Merz, G. E.; Moritz, M.; Nguyen, H. C.; Nowotny, C.; Puchades, C.; Rizo, A. N.; Schulze-Gahmen, U.; Smith, A. M.; Sun, M.; Young, I. D.; Zhao, J.; Asarnow, D.; Biel, J.; Bowen, A.; Braxton, J. R.; Chen, J.; Chio, C. M.; Chio, U. S.; Deshpande, I.; Doan, L.; Faust, B.; Flores, S.; Jin, M.; Kim, K.; Lam, V. L.; Li, F.; Li, J.; Li, Y.-L.; Li, Y.; Liu, X.; Lo, M.; Lopez, K. E.; Melo, A. A.; Moss, F. R.; Nguyen, P.; Paulino, J.; Pawar, K. I.; Peters, J. K.; Pospiech, T. H.; Safari, M.; Sangwan, S.; Schaefer, K.; Thomas, P. V.; Thwin, A. C.; Trenker, R.; Tse, E.; Tsui, T. K. M.; Wang, F.; Whitis, N.; Yu, Z.; Zhang, K.; Zhang, Y.; Zhou, F.; Trinidad, D.; Agard, D. A.; Cheng, Y.; Fraser, J. S.; Frost, A.; Jura, N.; Kortemme, T.; Manglik, A.; Southworth, D. R.; Stroud, R. M.; Rosenberg, O. S.; Verba, K. A.; Damas, J.; Hughes, G. M.; Keough, K. C.; Painter, C. A.; Persky, N. S.; Corbo, M.; Kirilenko, B.; Hiller, M.; Koepfli, K.-P.; Kaplow, I.; Wirthlin, M.; Pfenning, A. R.; Zhao, H.; Genereux, D. P.; Swofford, R.; Lind, A.; Pollard, K. S.; Ryderq, O. A.; Nweeia, M. T.; Meadows, J.; Dong, M.; Wallerman, O.; Marinescu, V.; Lindblad-Toh, K.; Ray, D. A.; Power, S.; Teeling, E. C.; Chauhan, G.; Li, S. X.; Karlsson, E. K.; Lewin, H. A. Comparative host-coronavirus protein interaction networks reveal pan-viral disease mechanisms. *Science* **2020**, *370*, No. eabe9403.

(12) Kim, D.-K.; Weller, B.; Lin, C.-W.; Sheykhkarimli, D.; Knapp, J. J.; Dugied, G.; Zanzoni, A.; Pons, C.; Tofaute, M. J.; Maseko, S. B.; Spirohn, K.; Laval, F.; Lambourne, L.; Kishore, N.; Rayhan, A.; Sauer, M.; Young, V.; Halder, H.; la Rosa, N. M.-d.; Pogoutse, O.; Strobel, A.; Schwehn, P.; Li, R.; Rothballer, S. T.; Altmann, M.; Cassonnet, P.; Coté, A. G.; Vergara, L. E.; Hazelwood, I.; Liu, B. B.; Nguyen, M.; Pandiarajan, R.; Dohai, B.; Coloma, P. A. R.; Poirson, J.; Giuliana, P.; Willems, L.; Taipale, M.; Jacob, Y.; Hao, T.; Hill, D. E.; Brun, C.; Twizere, J.-C.; Krappmann, D.; Heinig, M.; Falter, C.; Aloy, P.; Demeret, C.; Vidal, M.; Calderwood, M. A.; Roth, F. P.; Falter-Braun, P. A proteome-scale map of the SARS-CoV-2—human contactome. *Nat. Biotechnol.* **2023**, *41*, 140—149.

(13) Zhou, Y.; Liu, Y.; Gupta, S.; Paramo, M. I.; Hou, Y.; Mao, C.; Luo, Y.; Judd, J.; Wierbowski, S.; Bertolotti, M.; Nerkar, M.; Jehi, L.; Drayman, N.; Nicolaescu, V.; Gula, H.; Tay, S.; Randall, G.; Wang, P.; Lis, J. T.; Feschotte, C.; Erzurum, S. C.; Cheng, F.; Yu, H. A comprehensive SARS-CoV-2—human protein—protein interactome reveals COVID-19 pathobiology and potential host therapeutic targets. *Nat. Biotechnol.* **2023**, *41*, 128—139.

(14) Rao, V. S.; Srinivas, K.; Sujini, G. N.; Kumar, G. N. S. Protein-protein interaction detection: methods and analysis. *Int. J. Proteomics* **2014**, *2014*, 1—12.

(15) Peng, X.; Wang, J.; Peng, W.; Wu, F.-X.; Pan, Y. Protein—protein interactions: detection, reliability assessment and applications. *Briefings Bioinf.* **2016**, *18*, 798—819.

(16) Sierecki, E.; Giles, N.; Polinkovsky, M.; Moustaqil, M.; Alexandrov, K.; Gambin, Y. A cell-free approach to accelerate the study of protein—protein interactions in vitro. *Interface Focus* **2013**, *3*, No. 20130018.

(17) Guo, Z.; Johnston, W.; Kovtun, O.; Mureev, S.; Bröcker, C.; Ungermann, C.; Alexandrov, K. Subunit organisation of in vitro reconstituted HOPS and CORVET multisubunit membrane tethering complexes. *PLoS One* **2013**, *8*, e81534.

(18) Kovtun, O.; Mureev, S.; Jung, W.; Kubala, M. H.; Johnston, W.; Alexandrov, K. Leishmania cell-free protein expression system. *Methods* **2011**, *55*, 58—64.

(19) Johnston, W. A.; Alexandrov, K.Production of eukaryotic cell-free lysate from *Leishmania tarentolae*. In *Cell-Free Protein Synthesis: Methods and Protocols*; Springer, 2014; pp 1—15.

(20) Mureev, S.; Kovtun, O.; Nguyen, U. T.; Alexandrov, K. Species-independent translational leaders facilitate cell-free expression. *Nat. Biotechnol.* **2009**, *27*, 747—752.

(21) Gagoski, D.; Polinkovsky, M. E.; Mureev, S.; Kunert, A.; Johnston, W.; Gambin, Y.; Alexandrov, K. Performance benchmarking of four cell-free protein expression systems. *Biotechnol. Bioeng.* **2016**, *113*, 292—300.

(22) Wu, Y.; Cui, Z.; Huang, Y.-H.; de Veer, S. J.; Aralov, A. V.; Guo, Z.; Moradi, S. V.; Hinton, A. O.; Deuis, J. R.; Guo, S.; Chen, K.-E.; Collins, B. M.; Vetter, I.; Herzig, V.; Jones, A.; Cooper, M. A.; King, G. F.; Craik, D. J.; Alexandrov, K.; Mureev, S. Towards a generic prototyping approach for therapeutically-relevant peptides and proteins in a cell-free translation system. *Nat. Commun.* **2022**, *13*, No. 260.

(23) Johnston, W. A.; Moradi, S. V.; Alexandrov, K. Adaption of the Leishmania Cell-Free Expression System to High-Throughput Analysis of Protein Interactions. In *High-Throughput Protein Production and Purification*; Springer, 2019; pp 403—421.

(24) Moradi, S. V.; Johnston, W. A.; Parker, J.; Alexandrov, K. *Leishmania tarentolae* cell-free based approach for rapid anitbody-antigen interaction analysis. *Methods Enzymol.* **2021**, *659*, 391—409.

(25) PerkinElmer. User's guide to Alpha assays protein:protein interactions. https://www.perkinelmer.com/lab-solutions/resources/docs/009625A_01_GDE.pdf.

(26) Moradi, S. V.; Gagoski, D.; Mureev, S.; Walden, P.; McMahon, K.-A.; Parton, R. G.; Johnston, W. A.; Alexandrov, K. Mapping Interactions among Cell-Free Expressed Zika Virus Proteins. *J. Proteome Res.* **2020**, *19*, 1522—1532.

(27) Lee, J.; Worrall, L. J.; Vuckovic, M.; Rosell, F. I.; Gentile, F.; Ton, A.-T.; Caveney, N. A.; Ban, F.; Cherkasov, A.; Paetzel, M.; Strynadka, N. C. J. Crystallographic structure of wild-type SARS-CoV-2 main protease acyl-enzyme intermediate with physiological C-terminal autoprocessing site. *Nat. Commun.* **2020**, *11*, No. 5877.

(28) Roe, M. K.; Junod, N. A.; Young, A. R.; Beachboard, D. C.; Stobart, C. C. Targeting novel structural and functional features of coronavirus protease nsp5 (3CL(pro), M(pro)) in the age of COVID-19. *J. Gen. Virol.* **2021**, *102*, No. 001558.

(29) Kern, D. M.; Sorum, B.; Mali, S. S.; Hoel, C. M.; Sridharan, S.; Remis, J. P.; Toso, D. B.; Kotecha, A.; Bautista, D. M.; Brohawn, S. G. Cryo-EM structure of SARS-CoV-2 ORF3a in lipid nanodiscs. *Nat. Struct. Mol. Biol.* **2021**, *28*, 573—582.

(30) Flower, T. G.; Buffalo, C. Z.; Hooy, R. M.; Allaire, M.; Ren, X.; Hurley, J. H. Structure of SARS-CoV-2 ORF8, a rapidly evolving

https://doi.org/10.1021/acsomega.3c01625
ACS Omega 2023, 8, 25009—25019

immune evasion protein *bioExiv* 2021; Vol. *118* 2 DOI: 10.1101/2020.08.27.270637.
(31) Valcarcel, A.; Bensussen, A.; Álvarez-Buylla, E. R.; Díaz, J. Structural analysis of SARS-CoV-2 ORF8 protein: pathogenic and therapeutic implications. *Front. Genet.* **2021**, *12*, No. 693227.
(32) Zhang, Z.; Nomura, N.; Muramoto, Y.; Ekimoto, T.; Uemura, T.; Liu, K.; Yui, M.; Kono, N.; Aoki, J.; Ikeguchi, M.; et al. Structure of SARS-CoV-2 membrane protein essential for virus assembly. *Nat. Commun.* **2022**, *13*, No. 4399.
(33) Li, J.; Guo, M.; Tian, X.; Wang, X.; Yang, X.; Wu, P.; Liu, C.; Xiao, Z.; Qu, Y.; Yin, Y.; et al. Virus-host interactome and proteomic survey reveal potential virulence factors influencing SARS-CoV-2 pathogenesis. *Med* **2021**, *2*, 99−112.e7.
(34) Lin, S.; Chen, H.; Ye, F.; Chen, Z.; Yang, F.; Zheng, Y.; Cao, Y.; Qiao, J.; Yang, S.; Lu, G. Crystal structure of SARS-CoV-2 nsp10/nsp16 2′-O-methylase and its implication on antiviral drug design. *Signal Transduction Targeted Ther.* **2020**, *5*, No. 131.
(35) Klima, M.; Yazdi, A. K.; Li, F.; Chau, I.; Hajian, T.; Bolotokova, A.; Kaniskan, H. Ü.; Han, Y.; Wang, K.; Li, D.; et al. Crystal structure of SARS-CoV-2 nsp10−nsp16 in complex with small molecule inhibitors, SS148 and WZ16. *Protein Sci.* **2022**, *31*, No. e4395.
(36) Kirchdoerfer, R. N.; Ward, A. B. Structure of the SARS-CoV nsp12 polymerase bound to nsp7 and nsp8 co-factors. *Nat. Commun.* **2019**, *10*, No. 2342.
(37) Gao, Y.; Yan, L.; Huang, Y.; Liu, F.; Zhao, Y.; Cao, L.; Wang, T.; Sun, Q.; Ming, Z.; Zhang, L.; et al. Structure of the RNA-dependent RNA polymerase from COVID-19 virus. *Science* **2020**, *368*, 779−782.
(38) Lan, J.; Ge, J.; Yu, J.; Shan, S.; Zhou, H.; Fan, S.; Zhang, Q.; Shi, X.; Wang, Q.; Zhang, L.; Wang, X. Structure of the SARS-CoV-2 spike receptor-binding domain bound to the ACE2 receptor. *Nature* **2020**, *581*, 215−220.
(39) Zou, L.; Moch, C.; Graille, M.; Chapat, C. The SARS-CoV-2 protein NSP2 impairs the silencing capacity of the human 4EHP-GIGYF2 complex. *iScience* **2022**, *25*, No. 104646.
(40) Peacock, T. P.; Goldhill, D. H.; Zhou, J.; Baillon, L.; Frise, R.; Swann, O. C.; Kugathasan, R.; Penn, R.; Brown, J. C.; Sanchez-David, R. Y.; et al. The furin cleavage site in the SARS-CoV-2 spike protein is required for transmission in ferrets. *Nat. Microbiol.* **2021**, *6*, 899−909.
(41) Xia, S.; Liu, M.; Wang, C.; Xu, W.; Lan, Q.; Feng, S.; Qi, F.; Bao, L.; Du, L.; Liu, S.; Qin, C.; Sun, F.; Shi, Z.; Zhu, Y.; Jiang, S.; Lu, L. Inhibition of SARS-CoV-2 (previously 2019-nCoV) infection by a highly potent pan-coronavirus fusion inhibitor targeting its spike protein that harbors a high capacity to mediate membrane fusion. *Cell Res.* **2020**, *30*, 343−355.
(42) Jackson, C. B.; Farzan, M.; Chen, B.; Choe, H. Mechanisms of SARS-CoV-2 entry into cells. *Nat. Rev. Mol. Cell Biol.* **2022**, *23*, 3−20.
(43) Kim, D.-K.; Knapp, J. J.; Kuang, D.; Chawla, A.; Cassonnet, P.; Lee, H.; Sheykhkarimli, D.; Samavarchi-Tehrani, P.; Abdouni, H.; Rayhan, A.; et al. A comprehensive, flexible collection of SARS-CoV-2 coding regions. *G3: Genes, Genomes, Genet.* **2020**, *10*, 3399−3402.
(44) Galloway, S. E.; Paul, P.; MacCannell, D. R.; Johansson, M. A.; Brooks, J. T.; MacNeil, A.; Slayton, R. B.; Tong, S.; Silk, B. J.; Armstrong, G. L.; Biggerstaff, M.; Dugan, V. G. Emergence of SARS-CoV-2 B.1.1.7 Lineage — United States, December 29, 2020−January 12, 2021. *MMWR. Morb. Mortal. Wkly. Rep.* **2021**, *70*, 95−99.
(45) ECDC SARS-CoV-2 variants of concern as of 16 December 2021. https://www.ecdc.europa.eu/en/covid-19/variants-concern.
(46) Cheng, L.; Song, S.; Zhou, B.; Ge, X.; Yu, J.; Zhang, M.; Ju, B.; Zhang, Z. Impact of the N501Y substitution of SARS-CoV-2 Spike on neutralizing monoclonal antibodies targeting diverse epitopes. *Virol. J.* **2021**, *18*, No. 87.
(47) Liu, Y.; Liu, J.; Plante, K. S.; Plante, J. A.; Xie, X.; Zhang, X.; Ku, Z.; An, Z.; Scharton, D.; Schindewolf, C.; Widen, S. G.; Menachery, V. D.; Shi, P.-Y.; Weaver, S. C. The N501Y spike substitution enhances SARS-CoV-2 infection and transmission. *Nature* **2022**, *602*, 294−299.
(48) Gupta, D.; Sharma, P.; Singh, M.; Kumar, M.; Ethayathulla, A. S.; Kaur, P. Structural and functional insights into the spike protein mutations of emerging SARS-CoV-2 variants. *Cell. Mol. Life Sci.* **2021**, *78*, 7967−7989.
(49) Jhun, H.; Park, H.-Y.; Hisham, Y.; Song, C.-S.; Kim, S. SARS-CoV-2 Delta (B.1.617.2) Variant: A Unique T478K Mutation in Receptor Binding Motif (RBM) of Spike Gene. *Immune Network* **2021**, *21*, No. e32.
(50) Dalvie, N. C.; Rodriguez-Aponte, S. A.; Hartwell, B. L.; Tostanoski, L. H.; Biedermann, A. M.; Crowell, L. E.; Kaur, K.; Kumru, O. S.; Carter, L.; Yu, J.; et al. Engineered SARS-CoV-2 receptor binding domain improves manufacturability in yeast and immunogenicity in mice. *Proc. Natl. Acad. Sci.* **2021**, *118*, No. e2106845118.
(51) Gagoski, D.; Mureev, S.; Giles, N.; Johnston, W.; Dahmer-Heath, M.; Škalamera, D.; Gonda, T. J.; Alexandrov, K. Gateway-compatible vectors for high-throughput protein expression in pro-and eukaryotic cell-free systems. *J. Biotechnol.* **2015**, *195*, 1−7.
(52) Gadhave, K.; Kumar, P.; Kumar, A.; Bhardwaj, T.; Garg, N.; Giri, R. Conformational dynamics of 13 amino acids long NSP11 of SARS-CoV-2 under membrane mimetics and different solvent conditions. *Microb. Pathog.* **2021**, *158*, No. 105041.
(53) PerkinElmer Anti-GFP AlphaLISA protocol. https://www.perkinelmer.com/au/product/anti-gfp-alphalisa-acc-250-ug-al133c.

https://doi.org/10.1021/acsomega.3c01625
ACS Omega 2023, 8, 25009−25019